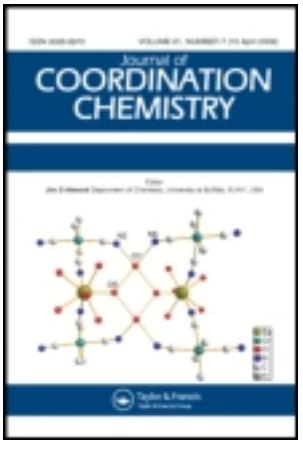

Journal of Coordination Chemistry
Publication details, including instructions for authors and subscription information:
http://www.tandfonline.com/loi/gcoo20

Vanadyl(IV) complexes of 4-alkoxy substituted [N,O] donor salicylaldimine Schiff bases derived from chloro-/nitro-aniline: synthesis, mesomorphism, and DFT study

Chira R. Bhattacharjee [a], Gobinda Das [a], Debraj Dhar Purkayastha [a], Prakash Kanoo [a] & Paritosh Mondal [a]
[a] Department of Chemistry, Assam University, Silchar 788011, Assam, India
Published online: 09 Aug 2011.

Journal of Coordination Chemistry
Vol. 64, No. 15, 10 August 2011, 2746–2760

Vanadyl(IV) complexes of 4-alkoxy substituted [N,O] donor salicylaldimine Schiff bases derived from chloro-/nitro-aniline: synthesis, mesomorphism, and DFT study

CHIRA R. BHATTACHARJEE*, GOBINDA DAS, DEBRAJ DHAR PURKAYASTHA, PRAKASH KANOO and PARITOSH MONDAL

Department of Chemistry, Assam University, Silchar 788011, Assam, India

(*Received 25 January 2011; in final form 20 June 2011*)

Oxovanadium(IV)-Schiff-base complexes, $[VOL_2]$ {L = N,N′-bis-(4-X-amino phenyl (4′-*n*-alkoxy)-salicylaldiminato), $n = 10, 18$; X = Cl, NO_2}, have been synthesized from the interaction of vanadyl (VO^{2+}) and the bidentate [N,O] donor in methanol/ethanol. The compounds were characterized by FT–IR, ^{1}H- and ^{13}C-NMR, FAB-mass spectra, elemental analyses, and solution electrical conductivity. Mesomorphic behavior of the ligands and their vanadyl complexes were probed by polarizing optical microscopy and differential scanning calorimetry. The compounds are thermally stable and exhibit enantiotropic smectic A mesomorphism over the temperature range of 57–231°C. The mesophase–isotropic transition temperatures for the complexes are much higher than the ligands. Melting and clearing points of the compounds did not show any definitive trend with regards to alkoxy chain length or electronegative substituent. Variable temperature magnetic susceptibility measurements of the vanadyl complexes clearly show the absence of exchange interactions among the vanadyl spin centers. Non-electrolytic natures of the complexes were shown by conductometric measurements. A ν(V=O) of ~970 cm^{-1} corroborated the absence of any V=O···V=O interactions. Density functional theory study carried out using DMol3 at BLYP/DNP level to determine the energy-optimized structure revealed a distorted square pyramidal geometry for the vanadyl complexes.

Keywords: Metallomesogen; Schiff bases; Vanadyl; DFT

1. Introduction

Vanadium complexes continue to be of interest because of their versatile physico-chemical properties, bioactivities, and catalytic properties in organic and inorganic transformations [1]. Coordination compounds of redox active metals that exhibit paramagnetism often undergo electronic excitations with visible light. Such properties can be exploited to produce conductors, magnetic materials, and display devices [2]. Oxovanadium(IV) complexes of Schiff-base ligands received significant attention for antimicrobial [3–5], antitumor [6], anti-leukemia [7], spermicidal [8], and insulin mimetic activities [9, 10]. Owing to unusual geometries, large birefringence, polarizability, and paramagnetism leading to unique functional behavior, metallomesogens incorporating

*Corresponding author. Email: crbhattacharjee@rediffmail.com

ISSN 0095-8972 print/ISSN 1029-0389 online © 2011 Taylor & Francis
DOI: 10.1080/00958972.2011.606461

vanadyl metal ions is an attractive option for current research [11–16]. Unlike other first-row transition metals, oxovanadium(IV) complexes form linear chain-like (–V=O–V=O–)*n* structures generating a polar order along the column axis [17]. Such a polar order is quite significant in the context of ferroelectric/piezoelectric and NLO materials [17]. Precise understanding and the control of phase behavior, though, is a function of chain length, substituents on the ligands, spacer groups, and nature of metal ions, making synthesis quite challenging [12, 18, 19]. Salicylaldimines have been exploited to access metal complexes with liquid crystalline properties [20–22]. Despite the inherent difficulties in synthesizing mesogenic vanadyl(IV) complexes, a number of vanadyl(IV) liquid crystalline complexes have been documented [23–31]. Due to paramagnetism induced by the VO(IV) center, such complexes show interesting chemical and physical properties [23–40]. Rich but complex mesomorphism exhibited by salicylaldimines and their metal complexes, including vanadium, has attracted considerable interest [32–34]. Oxovanadium(IV) complexes exhibit lower melting and clearing temperature compared to other transition metals. Very recently, our group reported a series of salen-type Schiff-base oxovanadium(IV) complexes that exhibit columnar/smectic mesomorphism [41–43]. In this article, we present the synthesis, characterization, and mesomorphism of new short-chain (C_{10}) and long-chain (C_{18}) bidentate rod-like [N,O] donor Schiff bases with 4-alkoxy substituent on the salicyldehyde ring with chloro- or nitro-substituents on the other phenyl ring and their vanadyl(IV) complexes.

2. Experimental

2.1. *Materials*

All solvents were purified and dried using standard procedures. The materials were procured from Tokyo Kasei and Lancaster Chemicals. Silica (60–120 mesh) from Spectrochem was used for chromatographic separation. Silica gel G (E-merck, India) was used for TLC.

2.2. *Techniques*

The C, H, and N analyses were carried out using a PE2400 elemental analyzer. Molar conductance of the compounds was determined in CH_2Cl_2 (*ca* 10^{-3} mol L^{-1}) at room temperature using an MAC-554 conductometer. ^{1}H-NMR spectra were recorded on a Bruker DPX-300 spectrometer in $CDCl_3$ solution with TMS as internal standard. Ultraviolet-visible absorption spectra in CH_2Cl_2 were recorded on a Shimadzu UV-160PC spectrophotometer. Infrared spectra were recorded on a Perkin Elmer L 120-000 A spectrometer as KBr discs. The mesomorphic texture of the compounds was studied using a polarizing microscope (Nikon optiphot-2-pol) attached with Instec hot- and cold-stage HCS302, STC200 temperature controller configured for HCS302. The accuracies in temperatures are 0.1°C. Thermal behavior of the compounds were studied using a Perkin Elmer differential scanning calorimeter (DSC) Pyris-1 spectrometer with a heating or cooling rate of 5°C min^{-1}. The magnetic measurements were made using SQUID equipment.

2.3. *Synthesis*

The general preparative route for salicylaldimine Schiff bases is presented in scheme 1. The two-step procedure involves alkylation of 2,4-dihydroxybenzaldehyde followed by condensation with *p*-chloro- or *p*-nitro-substituted aniline. The vanadyl(IV) complexes, VOL_2 (L = salicylaldimines), were synthesized by the interaction of hot ethanolic solution of the ligands and vanadyl sulfate in the presence of triethylamine under reflux (scheme 2). The bidentate [N,O] donor Schiff-base ligands were abbreviated as **1a-10**, **1a-18** (chloro substituted) and **1b-10**, **1b-18** (nitro substituted) and their complexes as **2a-10**, **2a-18** and **2b-10**, **2b-18** (**10** and **18** indicate the number of carbons in alkoxy chain).

2.4. *Synthesis of 4-n-octadecyloxysalicylaldehyde*

In this study, 2,4-dihydroxybenzaldehyde (2.7 g, 20 mmol), potassium bicarbonate (2 g, 20 mmol), potassium iodide (catalytic amount), and 1-bromooctadecane (6.1 g, 20 mmol) were mixed in 400 cm^3 dry acetone. The mixture was refluxed for 40 h and filtered when hot to remove insoluble solids. Dilute hydrochloric acid was added to neutralize the warm solution, which was then extracted twice with $CHCl_3$. The combined $CHCl_3$

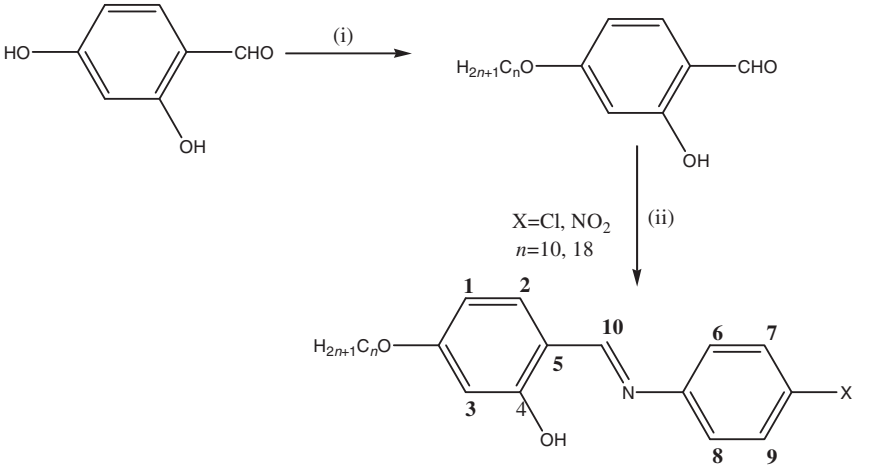

Scheme 1. (i) $C_nH_{2n+1}Br$, $KHCO_3$, KI, dry acetone, Δ, 40 h; (ii) glacial AcOH, absolute EtOH Δ, 4 h.

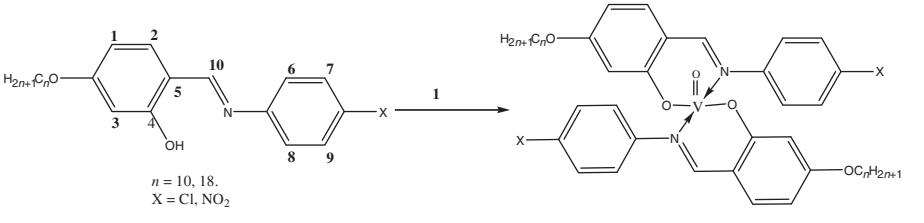

Scheme 2. (1) $VOSO_4 \cdot 5H_2O$, MeOH, TEA. Δ, 1 h.

extracts were concentrated to give a purple solid. The solid was purified by column chromatography with silica gel (100–200) mesh with a mixture of hexane: $CHCl_3$ (1 : 1). The solvent was evaporated to give a white solid product. Yield: 7.0 g, 80%. Anal. Calcd for $C_{25}H_{42}O_3$: FAB Mass (m/e, fragment): *m/z*: Calcd 390.3; Found: 391 $[M+H^+]$. ^{1}H-NMR (400 MHz, $CDCl_3$): 0.91(t, $J=5.7$, 6H, CH_3), 1.21–1.73(m, 30 H, $(CH_2)7$), 3.98(t, $J=5.9$, 2H, OCH_2), 7.4(d, $J=7.2$, 1H, H-aryl), 5.9(s, 1H, OH), and 10.9(s, 1H, –CHO); ^{13}C-NMR (75.45 MHz; $CDCl_3$; Me_4Si at 25°C, ppm) $\delta=107.3$ (–C1), 130.1 (–C2), 103.9 (–C3), 165.6 (–C4), and 189.8(–C10). IR (ν_{max}, cm^{-1}, KBr): 3424(νOH), 2913(ν_{as}(C–H), CH_3), 2914(ν_{as}(C–H), CH_2), 2867(ν_s(C–H), CH_3), 2847(ν_{as}(C–H), CH_2), 1625(ν(CH=O)), and 1278(ν(C–O)).

2.5. *Synthesis of 4-n-decyloxysalicylaldehyde*

In this study, 4-*n*-decyloxysalicylaldehyde was synthesized as described in section 2.4. Yield: 5 g, 86%. Anal. Calcd for $C_{17}H_{26}O_3$ (%): FAB Mass (m/e, fragment): *m/z*: Calcd 278.1; Found (%): 279$[M+H^+]$. ^{1}H-NMR (400 MHz, $CDCl_3$): 0.96(t, $J=5.7$, 6H, CH_3), 1.21–1.74(m, 30H, $(CH_2)7$), 3.97(t, $J=5.9$, 2H, OCH_2), 7.5(d, $J=7.2$, 1H, H-aryl), 5.9(s, 1H, OH), and 10.6(s, 1H, –CHO); ^{13}C-NMR (75.45 MHz; $CDCl_3$; Me_4Si at 25°C, ppm) $\delta=107.3$ (–C1), 131.1 (–C2), 103.9 (–C3), 165.6 (–C4), 188.8 (–C10). IR (ν_{max}, cm^{-1}, KBr): 3424(νOH), 2913(ν_{as}(C–H), CH_3), 2914(ν_{as}(C–H), CH_2), 2867(ν_s(C–H), CH_3), 2845(ν_{as}(C–H), CH_2), 1625(ν(CH=O)), and 1273(ν(C–O)).

2.6. *N-(4-n-octadecyloxysalicylidene)-4′-n-chloroaniline (1a-18)*

An ethanolic solution of (4-*n*-octadecyloxy)-salicylaldehyde (0.3 g, 1 mmol) was added to an ethanolic solution of 4-chloroaniline (0.1 g, 1 mmol). The solution mixture was refluxed with a few drops of acetic acid as catalyst for 3 h to yield the Schiff base N-(4-*n*-octadecyloxysalicylidene)-4′-*n*-chloroaniline. The solid was collected by filtration and recrystallized several times from absolute ethanol to give a pure compound. Yield: 0.4 g, 75%. Anal. Calcd for $C_{31}H_{46}ClNO_2$ (%): C, 74.4; H, 9.2; and N, 2.8. Found (%): C, 74.1; H, 9.3; N, 2.7; FAB Mass (m/e, fragment): *m/z*: Calcd 499.3; Found: 500$[M+H^+]$. ^{1}H-NMR (400 MHz, $CDCl_3$): 0.87(t, $J=5.7$, 6H, CH_3), 1.25–1.78(m, 30H, $(CH_2)15$), 3.95(t, $J=5.9$, 2H, OCH_2), 7.3(d, $J=7.2$, 1H, H-aryl), 13.06(s, 1H, OH), and 8.5(s, 1H, CH=N); ^{13}C-NMR (75.45 MHz; $CDCl_3$; Me_4Si at 25°C, ppm) $\delta=106.3$ (–C1), 131.1 (–C2), 104.9 (–C3), 161.6 (–C4), 109.3 (–C5), 122.7 (–C6), 132.1 (–C7), 122.6 (–C8), 131.4 (–C9), and 159.8 (–C10). IR (ν_{max}, cm^{-1}, KBr): 3421(νOH), 2912(ν_{as}(C–H), CH_3), 2917(ν_{as}(C–H), CH_2), 2869(ν_s(C–H), CH_3), 2845(ν_{as}(C–H), CH_2), 1610(ν(C=N)), and 1274(ν(C–O)).

2.7. *N-(4-n-decyloxysalicylidene)-4′-n-chloroaniline (1a-10)*

The Schiff base (4-*n*-octadecyloxysalicylidene)-4′-*n*-chloroaniline was synthesized by the same procedure as in section 2.6. Yield: 0.390 g, 75%. Anal. Calcd for $C_{23}H_{30}ClNO_2$ (%): C, 71.2; H, 7.7; and N, 3.6. Found (%): C, 71.1; H, 7.5; and N, 3.5; FAB Mass (m/e, fragment): *m/z*: Calcd 387.2; Found: 388$[M+H^+]$. ^{1}H-NMR (400 MHz, $CDCl_3$): 0.87(t, $J=7.2$, 6H, $–CH_3$), 1.25–1.58(m, 14H, $(–CH_2)7$), 4.02(t, $J=6.4$, 2H, $–OCH_2$),

8.29(d, $J = 8.0$, ^{1}H, H-aryl), 13.06(s, ^{1}H, OH), and 8.5(s, ^{1}H, –CH=N). IR (ν_{max}, cm^{-1}, KBr): 3424(νOH), 2913(ν_{as}(C–H), CH_3), 2918(ν_{as}(C–H), CH_2), 2869(ν_s(C–H), CH_3), 2845(ν_{as}(C–H), CH_2), 1603(ν(C=N)), and 1278(ν(C–O).

2.8. *N-(4-n-octadecyloxysalicylidene)-4′-n-nitroaniline (1b-18)*

The Schiff base, (4-*n*-octadecyloxysalicylidene)-4′-*n*-nitroaniline was synthesized by a similar procedure as in section 2.6. In this study, 4-nitroaniline was used instead of 4-chloroaniline. Yield: 0.418 g, 78%. Anal. Calcd for $C_{31}H_{46}N_2O_4$ (%): C, 72.9; H, 9.0; and N, 5.4. Found (%): C, 71.8; H, 9.1; and N, 5.3; FAB Mass (m/e, fragment): *m*/*z*: Calcd 510.3; Found: 511[$M + H^+$] ^{1}H-NMR (400 MHz, $CDCl_3$): 0.87(t, $J = 7.2$, 6H, CH_3), 1.25–1.58(m, 30H, $(CH_2)15$), 4.02(t, $J = 6.4$, 2H, OCH_2), 8.29(d, $J = 8.0$, 1H, H-aryl), 13.06(s, 1H, OH), and 8.5(s, 1H, CH=N); ^{13}C-NMR (75.45 MHz; $CDCl_3$; Me_4Si at 25°C, ppm) $\delta = 107.2$ (–C1), 130.1 (–C2), 102.4 (–C3), 161.5 (–C4), 109.8 (–C5), 122.9 (–C6), 122.3 (–C7), 123.6 (–C8), 122.4 (–C9), and 147.8 (–C10). IR (ν_{max}, cm^{-1}, KBr): 3435(νOH), 2917(ν_{as}(C–H), CH_3), 2919(ν_{as}(C–H), CH_2), 2869(ν_s(C–H), CH_3), 2845(ν_{as}(C–H), CH_2), 1603(ν(C=N)), 1278(ν(C–O)), 1516(ν_{as}(NO)), and 1350((ν_s(NO)).

2.9. *N-(4-n-decyloxysalicylidene)-4′-n-nitroaniline (1b-10)*

The Schiff base (4-*n*-octadecyloxysalicylidene)-4′-*n*-nitroaniline was synthesized by the same procedure as in section 2.6. Yield: 0.316 g, 76%. Anal. Calcd for $C_{23}H_{30}N_2O_4$ (%): C, 69.3; H, 7.5; and N, 7.0. Found (%): C, 70.1; H, 7.3; and N, 7.3; FAB Mass (m/e, fragment): *m*/*z*: Calcd 398.2; Found: 399[$M + H^+$]. ^{1}H-NMR (400 MHz, $CDCl_3$): 0.87(t, $J = 7.2$, 6H, CH_3), 1.25–1.58(m, 30H, (CH2)15), 4.02(t, $J = 6.4$, 2H, OCH_2), 8.29(d, $J = 8.0$, 1H, H-aryl), 13.06(s, 1H, OH), and 8.5(s, 1H, CH=N). IR (ν_{max}, cm^{-1}, KBr): 3433(νOH), 2915(ν_{as}(C–H), CH_3), 2917(ν_{as}(C–H), CH_2), 2867(ν_s(C–H), CH_3), 2844(ν_{as}(C–H), CH_2), 1602(ν(C=N)), 1276(ν(C–O)), 1516(ν_{as}(NO)), and 1351((ν_s(NO)).

2.10. *Synthesis of oxovanadium(IV) complexes*

The ligand **1a-18** (0.10 g, 0.2 mmol), **1a-10** (0.07 g, 0.2 mmol), **1b-18** (0.10 g, 0.2 mmol), or **1b-10** (0.08 g, 0.2 mmol) was dissolved in minimum absolute ethanol and vanadyl sulphate, $VOSO_4 \cdot 5H_2O$ (0.01 g, 0.1 mmol) dissolved in methanol was added to it followed by the addition of triethylamine and refluxed for 2 h. A greenish solid that formed immediately was filtered, washed with diethyl ether, and recrystallized from chloroform–ethanol.

2.10.1. Oxovanadium(IV) complex (2a-18). Yield: 0.08 g, 75%. Anal. Calcd for $C_{62}H_{90}Cl_2N_2O_5V$ (%): C, 69.9; H, 8.5; and N, 2.6. Found (%): C, 70.1; H, 8.3; and N, 2.5; FAB Mass (m/e, fragment): *m*/*z*: Calcd 1063.6; Found: 1064[$M + H^+$]. IR (ν_{max}, cm^{-1}, KBr): 2920(ν_{as}(C–H), CH_3), 2850(ν_{as}(C–H), CH_2), 1612(ν(C=N)), and 981(ν(V=O)).

2.10.2. Oxovanadium(IV) complex (2a-10). Yield: 0.06 g, 75%. Anal. Calcd for $C_{46}H_{58}Cl_2N_2O_5V$ (%): C, 65.7; H, 6.9; and N, 3.3. Found (%): C, 65.2; H, 6.8; and N, 3.1; FAB Mass (m/e, fragment): *m/z*: Calcd 839.3; Found: 840[M + H$^+$]. IR (ν_{max}, cm^{-1}, KBr): 2919(ν_{as}(C–H), CH_3), 2851(ν_{as}(C–H), CH_2), 1589(ν(C=N)), and 981(ν(V=O)).

2.10.3. Oxovanadium(IV) complex (2b-18). Yield: 0.08 g, 77%. Anal. Calcd for $C_{62}H_{90}N_4O_9V$ (%): C, 68.5; H, 8.3; and N, 5.1. Found (%): C, 68.1; H, 8.1; and N, 5.2; FAB Mass (m/e, fragment): *m/z*: Calcd 1085.6; Found: 1086[M + H$^+$]. IR (ν_{max}, cm^{-1}, KBr): 2919(ν_{as}(C–H), CH_3), 2851(ν_{as}(C–H), CH_2), 1584(ν(C=N)), and 991(ν(V=O)).

2.10.4. Oxovanadium(IV) complex (2b-10). Yield: 0.07 g, 79%. Anal. Calcd for $C_{46}H_{58}N_4O_9$ (%): C, 64.1; H, 6.7; and N, 6.5. Found (%): C, 64.2; H, 6.6; and N, 6.4; FAB Mass (m/e, fragment): *m/z*: Calcd 861.4; Found: 862[M + H$^+$]. IR (ν_{max}, cm^{-1}, KBr): 2920(ν_{as}(C–H), CH_3), 2850(ν_{as}(C–H), CH_2), 1595(ν(C=N)), and 988(ν(V=O)).

3. Results and discussion

The Schiff bases were obtained as yellow microcrystalline solids in good yields. The complexes were isolated as greenish solids in good yields and are readily recrystallized from methanol/CH_2Cl_2. The compounds were characterized by ^{1}H- and ^{13}C-NMR, FT–IR, FAB-mass spectrometry, UV-Vis spectroscopy, and elemental analysis.

Solution electrical conductivities of a typical ligand (**1a-10**) and complex (**2a-10**) recorded in CH_2Cl_2 (10^{-3} mol L^{-1}) were in the range 5.8–1.4 Ω^{-1} cm^{-1} mol^{-1}, much lower than 1 : 1 electrolytes [44], confirming the non-electrolytic nature of the complexes [16].

The shift of ν_{CN} vibrational stretching frequency at *ca* 1625 cm^{-1} to lower wavenumber ($\Delta\nu \sim 30$ cm^{-1}) and the absence of ν_{OH} (phenolic) mode upon chelation (table 1) clearly suggest the coordination of azomethine N and phenolate oxygen to the metal. The ν(C=N) is independent of the length of alkoxy side chain in both ligands and their complexes. The vanadyl(V=O) stretching at *ca* 980 cm^{-1} is suggestive of the absence of any intermolecular ($\cdots$V=O$\cdots$V=O$\cdots$) interaction, indicating the monomeric nature of the complexes. The presence of linear chain interactions usually causes ν(V=O) to shift to lower wavelengths (*ca* 870 cm^{-1}). IR data also show V=O stretching frequency to be insensitive to the length of the alkoxy side chain. Two weak bands in the low energy region (400–600 cm^{-1}) assignable to ν(M–N) and ν(M–O) provide compelling evidence for the coordination of metal in the ligand framework [16].

Electronic absorption spectra (figure 1) of the ligands (**1a-18**) exhibited bands at ~246 nm ($\varepsilon = 3400$ L mol^{-1} cm^{-1}), at ~295 ($\varepsilon = 2900$ L mol^{-1} cm^{-1}) due to π–π* intra-ligand transitions of the aromatic rings, and at ~337 nm ($\varepsilon = 5400$ L mol^{-1} cm^{-1}) for π–π* transitions of imine (–C=N) chromophores. The latter band is blue shifted to ~328 nm on complexation (figure 1). In addition, low intensity bands at ~400 nm ($\varepsilon = 2400$ L mol^{-1} cm^{-1}) for vanadyl(IV) complexes are assigned to MLCT transition. A weak shoulder at 450 nm in **2a-18** ($\varepsilon = 700$ L mol^{-1} cm^{-1}) is attributed

Table 1. Analytical and spectral data of the compounds.

Compounds	C(%)	H(%)	N(%)	UV-Vis λ_{max}(nm) (ε, L mol^{-1} cm^{-1}) (Transition)	IR(cm^{-1})	m/z(FAB$^+$)
$C_{31}H_{46}ClNO_2$ (**1a-18**)	74.1(74.4)	9.3(9.2)	2.7(2.8)	246(3500) ($\pi \rightarrow \pi^*$) 295(2900) ($\pi \rightarrow \pi^*$) 337(2400) ($\pi \rightarrow \pi^*$)	1626(νC=N) 3300(νOH)	500(499.3)
$C_{62}H_{90}Cl_2N_2O_5V$ (**2a-18**)	70.1(69.9)	8.3(8.5)	2.5(2.6)	245(5400) ($\pi \rightarrow \pi^*$) 328(2200) ($\pi \rightarrow \pi^*$) 400(2500) (MLCT) 450(700) (d–d)	1610(νC=N) 980(νV=O) 533(νM–N) 462(νM–O)	1064(1063.6)
$C_{23}H_{30}ClNO_2$ (**1a-10**)	71.1(71.2)	7.5(7.7)	3.5(3.6)	246(3600) ($\pi \rightarrow \pi^*$) 298(2700) ($\pi \rightarrow \pi^*$) 336(2400) ($\pi \rightarrow \pi^*$)	1627(νC=N) 3435(νOH)	388(387.2)
$C_{46}H_{58}Cl_2N_2O_5V$ (**2a-10**)	65.2(65.7)	6.8(6.9)	3.1(3.3)	244(5400) ($\pi \rightarrow \pi^*$) 328(2200) ($\pi \rightarrow \pi^*$) 398(2400) (MLCT) 449(650) (d–d)	1608(νC=N) 979(νV=O) 539(νM–N) 488(νM–O)	840(839.3)
$C_{23}H_{30}N_2O_4$ (**1b-10**)	69.2(69.3)	7.4(7.5)	7.1(7.0)	244(5400) ($\pi \rightarrow \pi^*$) 295(2900) ($\pi \rightarrow \pi^*$) 334(2400) ($\pi \rightarrow \pi^*$)	1621(νC=N) 3433(νOH)	399(398.2)
$C_{46}H_{58}N_4O_9V$ (**2b-10**)	64.2(64.1)	6.6(6.7)	6.4(6.5)	242(5300) ($\pi \rightarrow \pi^*$) 328(2400) ($\pi \rightarrow \pi^*$) 402(2400) (MLCT) 451(500) (d–d)	1595(νC=N) 988(νV=O) 530(νM–N) 486(νM–O)	862(861.4)
$C_{31}H_{46}N_2O_4$ (**1b-18**)	71.8(72.9)	9.1(9.0)	5.3(5.4)	246(3600) ($\pi \rightarrow \pi^*$) 300(2800) ($\pi \rightarrow \pi^*$) 336(2400) ($\pi \rightarrow \pi^*$)	1626(νC=N) 3435(νOH)	511(510.3)
$C_{62}H_{90}N_4O_9V$ (**2b-18**)	68.1(68.5)	8.1(8.3)	5.2(5.1)	244(5300) ($\pi \rightarrow \pi^*$) 328(2300) ($\pi \rightarrow \pi^*$) 398(2400) (MLCT) 455(400) (d–d)	1613(νC=N) 991(νV=O) 536(νM–N) 465(νM–O)	1086(1085.6)

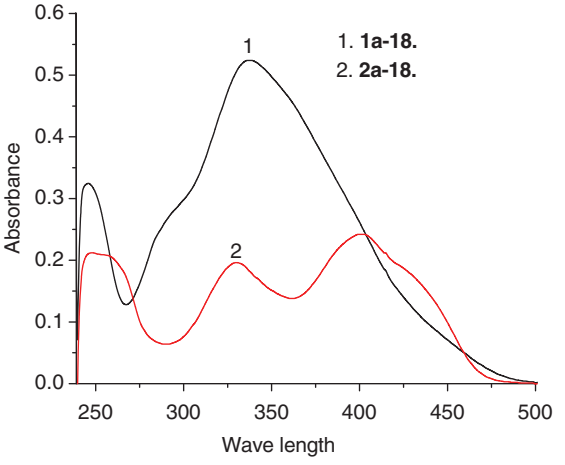

Figure 1. UV-Visible spectra of **1a-18** and **2a-18**.

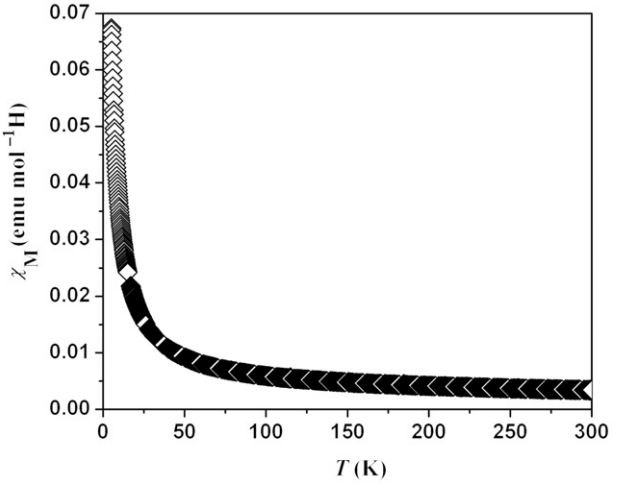

Figure 2. Variation of magnetic susceptibility of **2a-18** with temperature.

to d–d transition. A rather similar observation (table 1) was also noted for the nitro-substituted series [5, 16].

^{1}H-NMR spectra of ligands showed a signal at $\delta = 13.4$–13.8 ppm, corresponding to OH. The imine proton appeared at 8.5 ppm. Multiplets at 6.4–7.3 ppm are attributable to aromatic protons. The ^{13}C-NMR spectra for both ligands showed a signal at ~163 ppm, attributable to azomethine carbon. Carbons in the benzene ring showed signals at 102–151 ppm [5, 42–44].

3.1. *Variable temperature magnetic susceptibility study*

Variable temperature magnetic susceptibility measurements were carried out for a representative complex **2a-18** (figure 2). The compound follows the Curie–Weiss law.

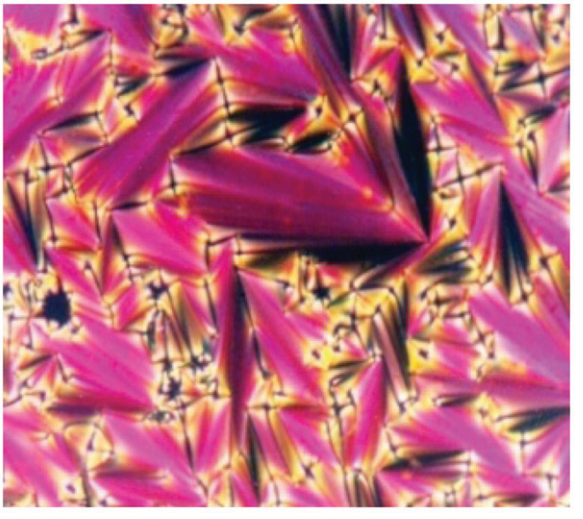

Figure 3. POM texture of **1a-10**.

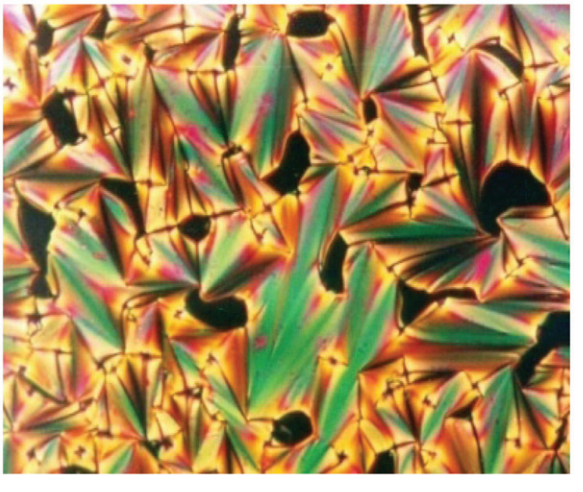

Figure 4. POM texture of **2a-10**.

Absence of a maximum in χ_M *versus* T led us to infer that there are no strong exchange interactions between the spin centers. Efficient super exchange is presumably hindered by the coordinating ability of the metal ion. Hence, the vanadium complexes can be considered as magnetically isolated spin centers.

3.2. *Mesomorphic properties*

Owing to the viscous nature of the complexes, DSC thermograms often did not show sharp peaks. Typical fan-like textures (figures 3 and 4) characteristic of SmA dominated the phase sequence of all the ligands and their complexes. Thermal data (table 2) show an interesting trend as a function of the electron-withdrawing substituent (Cl or NO_2)

Table 2. DSC data of the ligands and complexes.

Compound		T (°C)	Transition	ΔH (kJ mol^{-1})
1a-10	Heating	75.84	Cr–SmA	34.93
		120.93	SmA–I	4.68
	Cooling	119.25	I–SmA	4.69
		45.66	SmA–Cr	20.29
2a-10	Heating	107.84	Cr–Cr_1	4.80
		146.52	Cr_1–SmA	4.50
		233.70	SmA–I	8.42
	Cooling	231.56	I–SmA	4.31
1b-10	Heating	57.30	Cr–SmA	36.42
		104.80	SmA–I	9.10
	Cooling	82.97	I–SmA	29.99
		43.99	SmA–Cr	39.20
2b-10	Heating	124.14	Cr–SmA	18.76
		185.58	SmA–I	16.73
	Cooling	166.17	I–SmA	16.34
1a-18	Heating	57.37	Cr–Cr_1	2.93
		90.61	Cr_1–SmA	57.47
		96.55	SmA–I	2.01
	Cooling	95.69	I–SmA	3.22
		75.88	SmA–Cr_1	61.93
		50.61	Cr_1–Cr	62.22
2a-18	Heating	114.17	Cr–Cr_1	34.20
		116.69	Cr_1–SmA	8.16
		135.29	SmA–I	7.86
	Cooling	60.54	I–Cr	21.75
1b-18	Heating	57.20	Cr–Cr_1	1.51
		60.53	Cr_1–Cr_2	1.57
		78.89	Cr_2–Cr_3	16.21
		81.89	Cr_3–SmA	27.82
		116.57	SmA–I	2.60
	Cooling	116.37	I–SmA	2.77
		66.87	SmA–Cr_3	46.31
		44.04	Cr_3–Cr	5.49
2b-18	Heating	75.23	Cr–Cr_1	1.07
		157.24	Cr_1–SmA	35.11
		171.14	SmA–I	5.37
	Cooling	159.26	I–SmA	1.50
		139.91	SmA–Cr	20.63

and carbon chain length (C_{10} or C_{18}). For the C_{10} ligand, both melting and clearing points of chloro-substituted compound (**1a-10**) are about 20°C higher than the nitro-substituted compound (**1b-10**). For the corresponding complexes, the melting point of the chloro-substituted one (**2a-10**) is about 45°C lower while the clearing point is ~50°C higher than that of the nitro-substituted compound (**2b-10**). Quite different trend, however, was observed for the C_{18} ligand and its complexes. The melting points of both chloro- and nitro-substituted ligands were almost the same (~57.3°C) while the clearing point of the former was ~20°C lower than the latter. The nitro-substituted C_{10} ligand also melted at 57.3°C. In this case, therefore, neither the substituent nor the carbon chain length had any effect on the melting temperatures. The C_{18} complexes, on the

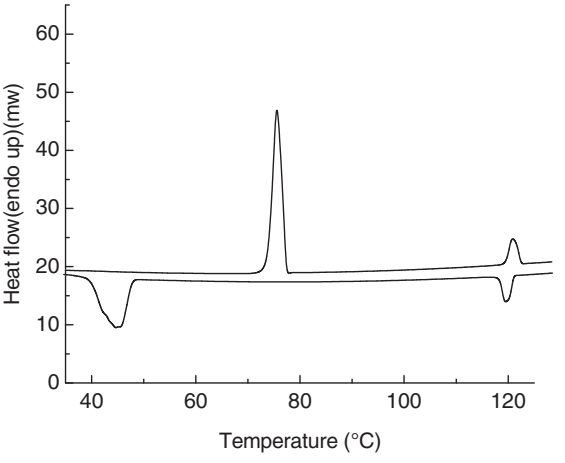

Figure 5. DSC thermogram of **1a-10**.

other hand, showed a difference of ~35°C between the chloro- and nitro-substituted ones, for both melting and clearing temperatures. On the whole, the melting temperatures of the complexes were always substantially higher than the ligands with no definitive trends with regards to chloro- or nitro-substituent or carbon chain length. Crystal-to-crystal phase transitions were often encountered and are one of the features of phase sequences observed for the compounds. The ligands and complexes all showed enantiotropic phase transitions. The enthalpies of transitions for $SmA \rightarrow I$ and *vice versa* for all the compounds are $<10\,kJ\,mol^{-1}$. For **1b-18**, as many as three low enthalpy crystal–crystal transitions could be seen on heating. The DSC thermogram for the typical compounds **1a-10** and **2a-10** are shown in figures 5 and 6.

3.3. *DFT study*

As efforts to obtain single crystals of the complexes failed, density functional theory (DFT) calculations are performed to investigate the electronic structure of the VO(IV) complexes (figures 7 and 8). Full geometry optimization of the complexes without symmetry constraint has been carried out with the DMol3 program package [45] using Kohn–Sham theory [46, 47]. The generalized gradient approximation (GGA) was used in the calculations. At the GGA level, we have chosen the BLYP functional [48, 49] which incorporates Becke's exchange and Lee–Yang–Parr correlation. The DNP basis functions, chosen in this study, are the double-numerical atomic orbitals augmented by polarization functions, i.e., functions with angular momentum one higher than that of the highest occupied orbital in the free atom [50]. The DNP basis set is believed to be more accurate than a Gaussian basis set 6-31G** of similar size. In our calculations, self-consistent field procedures are performed with a convergence criterion of 2×10^{-5} a.u. on the total energy and 10^{-6} a.u. on electron density. Highest occupied molecular orbital (HOMO) and lowest unoccupied molecular orbital (LUMO) diagrams of the complexes **2a-10** and **2b-10** are shown in figures 9(a), (b) and 10(a), (b), respectively. In both complexes, electron density of the HOMO is localized mainly

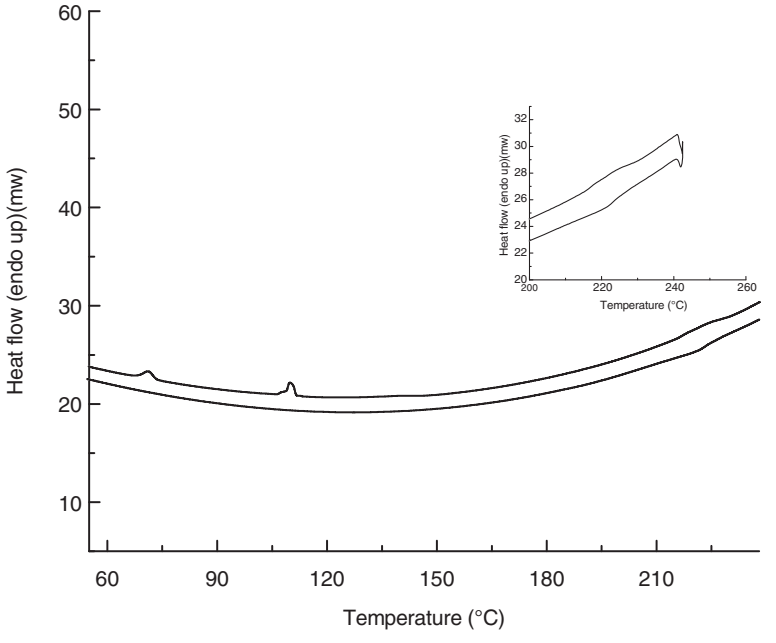

Figure 6. DSC thermogram of **2a**-**10**.

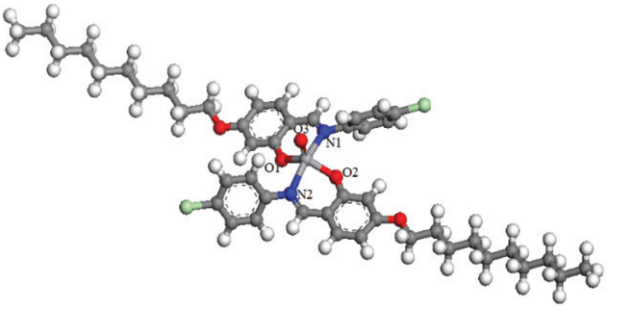

Figure 7. DFT optimized structure of **2a**-**10**.

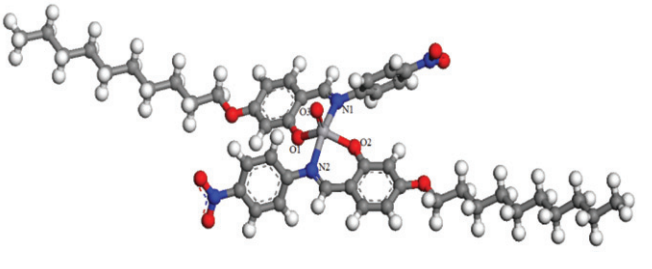

Figure 8. DFT optimized structure of **2b**-**10**.

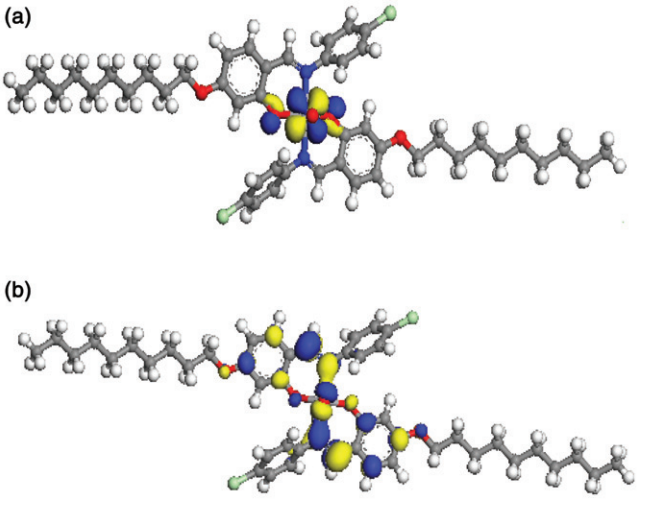

Figure 9. (a) HOMO of **2a-10** and (b) LUMO of **2a-10**.

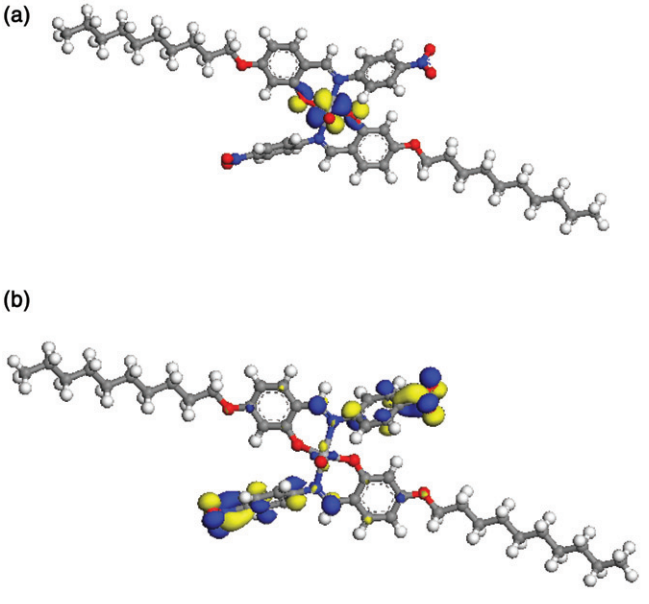

Figure 10. (a) HOMO of **2b-10** and (b) LUMO of **2b-10**.

on the vanadium while the LUMO of **2a-10** is localized on the alkoxy chain bearing the aromatic ring and that of **2b-10** is distributed on the nitro-substituted aromatic ring. Noticeable differences in the distribution of electron density on the LUMO of **2a-10** and **2b-10** may be ascribed to the electronegative substituents (–Cl and $–NO_2$). The molecular orbital energies of HOMO and LUMO of **2a-10** are calculated to be −4.18 eV and −2.59 eV, respectively, $\Delta E = 1.59$ eV. Corresponding energies for **2b-10** were −4.58 eV and −3.44 eV, $\Delta E = 1.14$. Some geometric parameters of optimized vanadium

Table 3. Selected bond lengths and angles of **2a-10** and **2b-10**.

Structure parameter	**2a-10**[a]	**2b-10**[a]
V–O(3)	1.622	1.621
V–O(1)	1.951	1.948
V–O(2)	1.952	1.948
V–N(1)	2.178	2.178
V–N(2)	2.177	2.176
O(1)–V–O(2)	129.5	129.5
N(1)–V–N(2)	161.9	161.9
N(1)–V–O(2)	86.2	86.3
O(1)–V–N(1)	86.2	86.1
O(1)–V–N(2)	86.0	85.9
N(2)–V–O(2)	86.2	86.2

[a]Bond lengths and angles are in Å and degrees, respectively.

complexes, evaluated by DFT calculation at BLYP/DNP level, are shown in table 3. The calculated bond distances of the complexes are in agreement with a related structurally characterized $[N_2O_2]$ donor bis(salicylaldiminato)vanadyl complex [16]. The bond angles of 129.5° and 161.9° for O1–V–O2 and N1–V–N2, respectively, in both complexes suggest a distorted square pyramidal geometry. Theoretical (DFT) calculations show that the enol form (−42.61 eV) of the ligand is relatively more stable than the keto form (−42.43 eV), hence coordination in enol form appears more plausible.

4. Conclusions

New rod-shaped Schiff bases with a short and long 4-alkoxy chain at one end and chloro or nitro at the other were prepared. Low conductivity values confirm the complexes as non-electrolytes. The ligands show enantiotropic SmA phases *via* batonnets over a temperature range 57–120°C. The complexes also show enantiotropic SmA phase but with a higher transition temperature than those of the corresponding ligands. Some of the complexes showed crystal–crystal transitions, though only in the heating run. The phase transition temperatures of the C_{10} group of compounds were higher than those of C_{18}. Based on the spectral results, a five-coordinate square pyramidal structure has been speculated. Variable temperature magnetic susceptibility studies suggested isolated spin centers with no exchange interaction. The ν(V=O) band at 970 cm^{-1} also suggested the lack of discernible intermolecular $\cdots$V=O$\cdots$V=O$\cdots$ interaction.

Acknowledgments

The authors thank SAIF, NEHU, and CDRI, Lucknow, for providing analytical and spectral data. G. Das acknowledges the financial support from DST and UGC, Government of India. Dr R.C. Deka, Tezpur University, India, is acknowledged for providing the computational facility.

References

[1] Y. Abe, A. Iyoda, K. Seto, A. Moriguchi, H. Yokoyama. *Eur. J. Inorg. Chem.*, 2148 (2008).
[2] Yu.G. Galyametdinov, I.G. Bikchantaev, I.V. Ovchinnikov. *Zh. Obshch. Khim.*, **58**, 1326 (1988).
[3] A. Butler, J.V. Walker. *Chem. Rev.*, **93**, 1937 (1993).
[4] N. Muhammad, S. Ali, S. Shahzadi, A.N. Khan. *Russ. J. Coord. Chem.*, **34**, 448 (2008).
[5] Z.H. Chohan, S.H. Sumrra, M.H. Youssoufi, T.B. Hadda. *J. Coord. Chem.*, **63**, 3981 (2010).
[6] P. Noblia, M. Vieites, B.S. Parajon-Costa, E.J. Baran, H. Cerecetto, P. Draper, M. Gonzalez, O.E. Piro, E.E. Castellano, A. Azqueta, A. Lopez de Cerain, A. Monge-Vega, D. Gambino. *J. Inorg. Biochem.*, **99**, 443 (2005).
[7] Y. Dong, R.K. Narla, E. Sudbeck, F.M. Uckun. *J. Inorg. Biochem.*, **78**, 321 (2000).
[8] O.J. D'Cruz, Y. Dong, F.M. Uckun. *Biol. Reprod.*, **60**, 435 (1999).
[9] H. Sakurai, Y. Kojitane, Y. Yoshikawa, K. Kawabe, H. Yasui. *Coord. Chem. Rev.*, **226**, 187 (2002).
[10] A. Butler, C.J. Carrano. *Coord. Chem. Rev.*, **109**, 61 (1991).
[11] P. Espinet, M.A. Esteruelas, L.A. Oro, J.L. Serrano, E. Sola. *Coord. Chem. Rev.*, **117**, 215 (1992).
[12] N. Hoshino. *Coord. Chem. Rev.*, **174**, 77 (1998).
[13] R. Paschke, D. Balkow, E. Sinn. *Inorg. Chem.*, **41**, 1949 (2002).
[14] N. Hoshino, H. Murakami, Y. Matsunaga, T. Inbe, Y. Maruyama. *Inorg. Chem.*, **29**, 1177 (1990).
[15] N. Hoshino, A. Kodama, T. Shibuya, Y. Matsunaga, S. Miyajima. *Inorg. Chem.*, **30**, 3091 (1991).
[16] M. Bagherzadeh, M. Amini. *J. Coord. Chem.*, **63**, 3849 (2010).
[17] Yu.G. Galyametdinov, I.G. Bikchantaev, I.V. Ovchinnikov. *Zh. Obshch. Khim.*, **58**, 1326 (1988).
[18] J.L. Serrano. *Metallomesogens*, Wiley-VCH, Weinheim (1996).
[19] B. Donnio, D Guillon, R. Deschenaux, D.W. Bruce. In *Comprehensive Coordination Chemistry II*, J.A. McCleverty, T.J. Meyer (Eds), pp. 357–627, Elsevier, Oxford (2003).
[20] I.V. Ovchinnikov, Yu.G. Galyametdinov, G.I. Ivanova, L.M. Yagfarova. *Dokl. Akad. Nauk. SSSR*, **276**, 1984 (126).
[21] Yu.G. Galyametdinov, G.I. Ivanova, I.V. Ovchinnikov. *Zh. Obshch. Khim.*, **54**, 2796 (1984).
[22] I.V. Ovchinnikov, Yu.G. Galyametdinov, I.G. Bikchantaev. *Izv. Akad. Nauk. SSSR, Ser. Fiz.*, **53**, 1870 (1989).
[23] J. Sleven, T. Cardinaels, K. Binnemans, D. Guillon, B. Donnio. *Liq. Cryst.*, **29**, 1425 (2002).
[24] J. Barbera, R. Gimenez, J.L. Serrano, P.J. Alonso, J.I. Martinez. *Chem. Mater.*, **15**, 958 (2003).
[25] A. Serrette, P.J. Carroll, T.M. Swager. *J. Am. Chem. Soc.*, **114**, 1887 (1992).
[26] A.B. Blake, J.R. Chipperfield, W. Hussain, R. Paschke, E. Sinn. *Inorg. Chem.*, **34**, 1125 (1995).
[27] E. Meyer, C. Zucco, H. Gallardo. *J. Mater. Chem.*, **8**, 1351 (1998).
[28] A.G. Serrette, T.M. Swager. *J. Am. Chem. Soc.*, **115**, 8879 (1993).
[29] M.A. Perez-Jubindo, M.R. De La Fuente, M. Marcos. *Adv. Mater.*, **6**, 941 (1994).
[30] M. Marcos, J.L. Serrano. *Adv. Mater.*, **3**, 256 (1991).
[31] P.J. Alonso, M.L. Sanjuan, P. Romero, M. Marcos, J.L. Serrano. *J. Phys. Condens. Mater.*, **2**, 9173 (1990).
[32] Yu.G. Galyametdinov, I.G. Bikchantaev, I.V. Ovchinnikov. *Zh. Obshch. Khim.*, **58**, 1326 (1988).
[33] W. Pyzuk, A. Krowczynski, L. Chen, E. Gorecka, I. Bickczantaev. *Liq. Cryst.*, **9**, 675 (1995).
[34] M. Ghedini, S. Morrone, R. Bartolino, V. Formoso, O. Francescangeli, B. Yang, D. Gatteschi, C. Znachini. *Chem. Mater.*, **5**, 876 (1993).
[35] H. Zheng, C.K. Lai, T.M. Swager. *Chem. Mater.*, **6**, 2252 (1994).
[36] H. Zheng, C.K. Lai, T.M. Swager. *Chem. Mater.*, **7**, 2067 (1995).
[37] Y. Abe, K. Nakabayashi, N. Matsukawa, M. Iida, T. Tanase, M. Sugibayashia, K. Ohta. *Inorg. Chem. Commun.*, **7**, 580 (2004).
[38] I. Aiello, M. Ghedini, F. Neve, D. Pucci. *Chem. Mater.*, **9**, 2107 (1997).
[39] K. Nejati, Z. Rezvani. *New J. Chem.*, **27**, 1665 (2003).
[40] Y. Abe, K. Nakabayashi, N. Matsukawa, H. Takashima, M. Iida, T. Tanase, M. Sugibayashi, H. Mukai, K. Ohta. *Inorg. Chim. Acta*, **359**, 3934 (2006).
[41] C.R. Bhattacharjee, G. Das, P. Mondal, S.K. Prasad, D.S.S. Rao. *Inorg. Chem. Commun.*, **14**, 606 (2011).
[42] C.R. Bhattacharjee, G. Das, P. Mondal, S.K. Prasad, D.S.S. Rao. *Liq. Cryst.*, **38**, 615 (2011).
[43] C.R. Bhattacharjee, G. Das, D.D. Purkayastha, P. Mondal. *Liq. Cryst.*, **38**, 717 (2011).
[44] W.J. Geary. *Coord. Chem. Rev.*, **7**, 81 (1971).
[45] B. Delley. *J. Chem. Phys.*, **92**, 508 (1990).
[46] P. Hohenberg, W. Kohn. *Phys. Rev. B*, **136**, 864 (1964).
[47] W. Kohn, L. Sham. *Phys. Rev. A*, **140**, 1133 (1965).
[48] A.D. Becke. *Phys. Rev. A*, **38**, 3098 (1988).
[49] C. Lee, W. Yang, R.G. Parr. *Phys. Rev. B*, **37**, 785 (1988).
[50] B. Delly, D.E. Ellis. *J. Chem. Phys.*, **76**, 1949 (1982).